Proceedings of the IASS 2024 Symposium
Redefining the Art of Structural Design
August 26-30, 2024, Zurich Switzerland
Philippe Block, Giulia Boller, Catherine DeWolf,
Jacqueline Pauli, Walter Kaufmann (eds.)

Non-developable surface structures using bilayer auxetic material and kerf bending joints

Kazuki HAYASHI*, Romain MESNIL[a]

*Kyoto University / École nationale des ponts et chaussées
Kyotodaigaku-katsura, Nishikyo, Kyoto 615-8540, Japan
hayashi.kazuki@archi.kyoto-u.ac.jp

[a] École nationale des ponts et chaussées

Abstract

Auxetic materials possess a unique characteristic known as a negative Poisson's ratio: the structure can expand in two in-plane directions subject to stretch. This property allows auxetic materials to achieve non-developable surface shapes and has been used in various small-scale products. However, this technique is rarely used in large-scale structures due to the requirement for joints with high deformation capacity for deployment, which also leads to excessive flexibility. To address these challenges, we introduce kerf patterns at the joints, ensuring the deployment process is within the elastic range. Additionally, we introduce an overlaying scheme for surface stiffening, where two auxetic surfaces with the same topology are attached. These improvements allow for using wood materials to create large-scale auxetic surface structures. Despite its geometric complexity, we have semi-automated the design and analysis processes, making auxetic materials more accessible.

Keywords: auxetic structures, meta-material, kerf bending, conformal mapping, discrete differential geometry

1. Introduction

Deployable structures with a flat initial configuration are of practical interest in the domain of architectural design and structural engineering since they can significantly reduce the workload and cost of fabrication, transport and construction. In combination with digital fabrication techniques, numerous researchers have tried to put the deployable structures into practice, which yielded new typologies of deployable structures inspired by origami [1], kirigami [2], material programming [3], etc.

Auxetic materials can also be regarded as a deployment method to achieve a target 3D shape from a 2D state. They are characterized by negative Poisson's ratio, a property rarely found in natural materials. Unlike traditional materials such as metals, polymers or woods, the term *material* in auxetic materials encompasses any substance that exhibits this unique deformation feature.

It is noteworthy that surfaces achieved by auxetic materials are not limited to developable surfaces; even non-developable surfaces can be realized through variable expansions across the surface. Owing to intriguing links between the cut pattern and deployed geometry, the study of auxetic materials has become interdisciplinary, involving computer graphics and discrete differential geometry [4,5].

Despite the active involvement of researchers with various backgrounds, most existing studies of auxetic materials investigate their mechanical properties at a smaller scale. Thus, the application of auxetic materials has been limited to small-scale products. Without a clear understanding of their underlying mechanical properties, the deployment and stabilization of auxetic materials are forced to rely on brute force methods, which makes the deployment result and the structural performance of the deployed state

too unpredictable. When applying auxetic materials to structures of a shelter scale or even larger, understanding their mechanical properties becomes more crucial for the sake of safety.

After overviewing the geometric properties of auxetic materials, this study first determines the necessary conditions for the material and auxetic cut pattern to remain within the elastic range during deployment. It is observed that the elastic conditions are too strict for auxetic materials with conventional cut patterns due to limited deformation capacity at the joints. Furthermore, we ascertain that the deployed structure cannot withstand external loads due to its excessive flexibility.

This study addresses these problems by introducing kerf bending, a technique to add material flexibility by a series of cuts [6], at the joints and overlaying two auxetic materials [7]. The kerf joints augment the deformation capacity necessary for deployment, and the overlaying scheme improves the structural stability of the deployed state. Furthermore, we develop the parametric design workflow of bilinear auxetic materials with kerf joints, and we demonstrate its effectiveness through physical prototyping.

2. Connection between auxetic materials and conformal flattening

2.1. Auxetic materials

Figure 1 shows a typical unit cell of auxetic material with an equilateral triangular pattern; two adjacent faces are connected at their corners, allowing them to rotate around the corner during the deployment process. Suppose the auxetic material is stretched in one direction while preserving geometric periodicity. In that case, the material is stretched in the perpendicular in-plane direction with the same amount, i.e., the Poisson's ratio of the auxetic material with an equilateral triangular pattern is -1.

Assuming the rigidity of unit cells and the zero-length hinge at the corner connections, the change in the size of the unit cell is associated only with the deployment angle $\theta \in [0, 2\pi/3]$: an open angle between two adjacent faces. Let the completely closed state, i.e., the left state of Fig. 1, be the initial configuration with zero strain, then the strain ε is expressed as

$$\varepsilon = 2\cos\left(\frac{\pi}{3} - \frac{\theta}{2}\right) - 1 \tag{1}$$

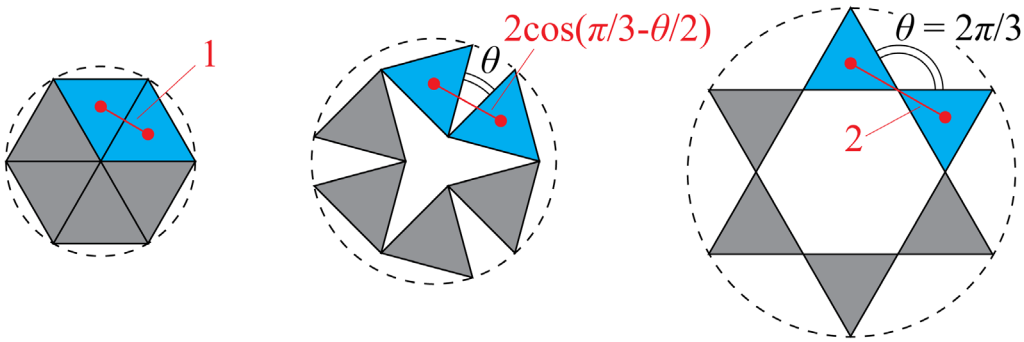

Figure 1: A unit cell of auxetic material with an equilateral triangular pattern

2.2. Geometric connection between auxetic materials and conformal mapping

Conformal mapping is a mathematical technique to transform a geometry while preserving angles, but not necessarily length scales. Especially when the conformal map flattens a 3D surface onto a 2D space, the process is called conformal flattening. Besides the flattened surface, conformal flattening algorithms compute conformal factors, which indicate pointwise in-plane expansion to achieve the original surface.

To explain the expansion in the context of conformal flattening in more detail, we introduce *metric* g, a notion of the area measurement across the surface. If the angles are preserved in a flattening process, the surface metrics at a corresponding point before and after the transformation, denoted by g_{3D} and $\tilde{g}_{2D}$, are related by

$$g_{3D} = e^{2u}\tilde{g}_{2D} \tag{2}$$

where u is called a log-conformal factor. Equation (2) can be interpreted as follows: to achieve the original 3D shape from the 2D shape by surface stretching, the infinitesimal area around the point needs to increase from 1 to e^{2u}. Assuming isometric area expansion, the axial strains in two orthogonal in-plane directions are both described as

$$\varepsilon = e^{u} - 1 \tag{3}$$

Among various methods for conformal flattening, the following method based on the generalized discrete Ricci flow [8] is used in this study. First, the generalized discrete Ricci flow optimizes the Ricci energy for the design surface in a triangular mesh format. From this optimization, we can obtain the log-conformal factors at the vertices and the edge lengths of the flattened state. Then, the flattened shape can be constructed from the edge lengths using the Euclidian law of cosines. See Ref. [8] for more details.

The shape of deployed auxetic material can be inferred from the conformally flattened shape of the target surface. By relating the strains obtained in Eq. (1) and Eq. (3), the deployment angle θ and the log-conformal factor u hold the following geometrical relationship:

$$2\cos\left(\frac{\pi}{3} - \frac{\theta}{2}\right) = e^{u} \tag{4}$$

Considering that θ is geometrically within the range $[0, 2\pi/3]$, the admissible range of u for the auxetic material is $[0, \log 2] \fallingdotseq [0, 0.693]$.

3. Structural performance-aware design of auxetic materials

3.1. Kerf bending joints

3.1.1. Strict elastic design constraints for conventional joints

For simplicity, the joint of conventional auxetic material is regarded as a short and thick beam with the length L, Young's modulus E, and the second moment of inertia I. The bending moment M required to cause the deployment angle θ by the beam flexure is expressed as

$$M = \frac{EI\theta}{L} \tag{5}$$

Assuming the beam cross-section is rectangular and the thickness of auxetic material is t, i.e., $I/Z = t/2$, the bending stress σ_{b} is

$$\sigma_{\mathrm{b}} = \frac{Et\theta}{2L} \tag{6}$$

To ensure the feasibility of the deployment in view of the elastic limit of the material, the bending stress σ_{b} must not exceed the elastic limit stress $\bar{\sigma}$.

The next step is to derive the relationship between the non-dimensional slenderness parameter of the beam L/t and the non-dimensional material parameter $E/\bar{\sigma}$.

$$\frac{L}{t} > \frac{\theta}{2} \cdot \frac{E}{\bar{\sigma}} \tag{7}$$

The parameter $E/\bar{\sigma}$ can be utilized as an indicator of material deformability; the material has higher deformability if $E/\bar{\sigma}$ is smaller [9]. Let grass fibre-reinforced polymers (GFRP) be the material to be used. From Ref. [10], its material properties are roughly assumed as $E = 15.0$ [GPa] and $\bar{\sigma} = 250.0$ [MPa]. Suppose the deployment angle θ is $\pi/3$, the necessary slenderness, $L_{\mathrm{GFRP}}/t_{\mathrm{GFRP}}$, for the joint made of GFRP is

$$\frac{L_{\mathrm{GFRP}}}{t_{\mathrm{GFRP}}} > 10\pi \fallingdotseq 31.4 \tag{8}$$

which is too strict to achieve. As grass fibre reinforced polymers (GFRP) have higher deformability than traditional materials like wood, steel, and concrete with respect to $E/\bar{\sigma}$ [9], the necessary slenderness

condition Eq. (8) becomes even more severe for traditional materials. This fact necessitates an additional solution to increase the joint flexibility.

3.1.2. Augmenting joint flexibility through kerfs

We consider relaxing the necessary slenderness condition at the joints by means of kerf bending. The parameters of the kerf shape are described in Fig. 2. The kerf shape parameters consist of the interval b, the depth h, and n which determines the number of kerfs. The compressive zone caused by deployment includes wedge-shaped cuts that prevent extra forces due to contact until reaching $\theta = \pi/3$.

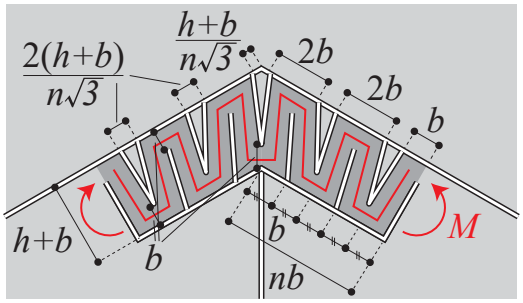

Figure 2: Notations for the proposed kerf joint

For simplicity, we assume that

- h is sufficiently larger than b so that the kerf joint is regarded as a set of linear beam elements along the load path.
- The second moment of inertia and the section modulus of the beam elements in the in-plane bending direction are uniformly expressed as $b^3t/12$ and $b^2t/6$, respectively.
- The tip nodes are subject to pure in-plane bending moment M, and no other external forces are considered.
- The total length of beam elements corresponding to the kerf joint is $2nh + (2n-1)b$, which is slightly shorter than the actual centre load path.

On this assumption, the bending moment required to cause the target deployment angle is obtained by the principle of virtual work as

$$M = \frac{Eb^3t}{24nh+(24n-12)b}\theta \tag{9}$$

The bending stress is obtained as

$$\sigma_{\mathrm{b}} = \frac{E\theta}{4n\frac{h}{b}+4n-2} \tag{10}$$

Similarly to Sec. 3.1.1, the relationship between the kerf parameters (b, h and n) and the non-dimensional material parameter $E/\bar{\sigma}$ is expressed as

$$4n\frac{h}{b} + 4n - 2 > \theta \cdot \frac{E}{\bar{\sigma}} \tag{11}$$

Figure 3 relates the non-dimensional material parameter E/σ_{b} to the kerf parameters. The kerfs allow polymer materials for the joints without strict constraints on the kerf parameters n and h/b. Although using wood materials is more challenging than using polymers, increasing the value of n makes it possible to use auxetic materials made of wood. Note that using a target surface with low curvatures, i.e., smaller deployment angle θ, can relax the constraint for the kerf parameters.

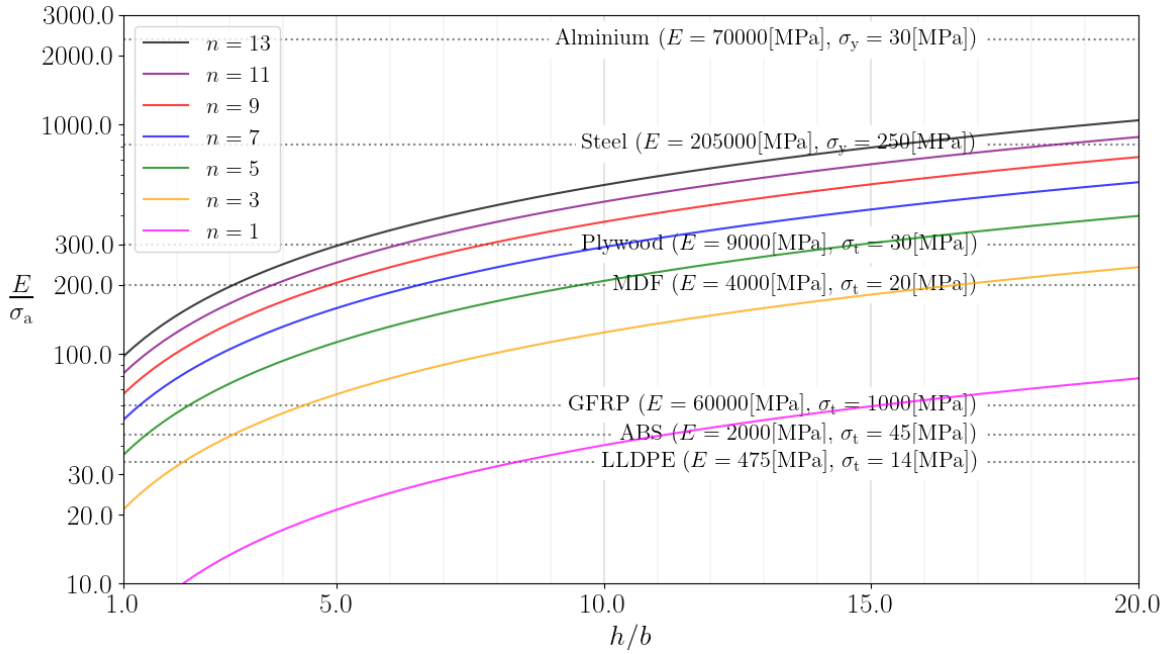

Figure 3: Parametric study of kerf shapes and the minimum requirement for various materials ($\theta = \pi/3$)

3.2. Overlaying auxetic materials

3.2.1. Over-flexibility of the deployed shape

This section discusses the over-flexibility problem of the deployed shape using an example. Suppose covering a circular area of 100.00 [m^2] without any supports inside. The target surface (the left side of Fig .5) is spherical, and its rise-to-span ratio is $1/6$. After the conformal flattening, an equilateral triangular mesh with a unit edge length of 1.0 m is defined onto the flattened shape as shown in the middle of Fig. 4. The deployed shape can be obtained by solving the optimization problem formulated by Konaković et al. [4] The weight parameters of the objective function (Eq. (2) of Ref. [4]) are fixed to $w_1 = 0.1$, $w_2 = 1.0$, and $w_3 = 1.5$, and the number of iterations is 100. The deployed shape after the optimization, shown on the right side of Fig. 4, closely matches the target shape.

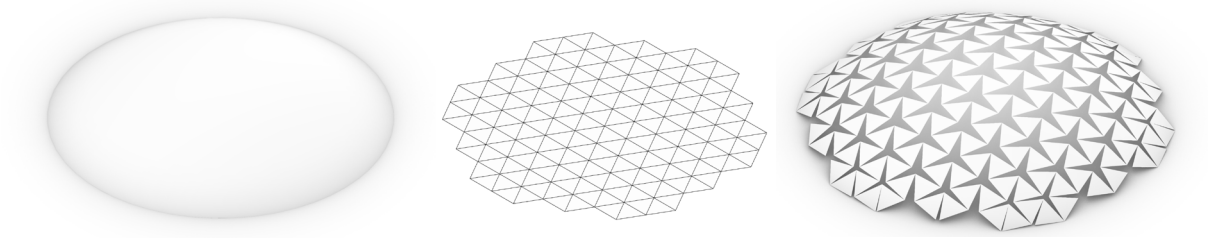

Figure 4: Target shape (left), equilateral triangular mesh (middle), and its deployed shape (right)

The deployed auxetic material stores elastic strain energy, and restoring forces occur that try to return it to its original shape. However, the restoring forces are disregarded for simplicity in this subsection; the deployed state holds its shape as long as no dead/live loads are applied. The method for holding the deployed shape is addressed in the next subsection.

The other parameters and settings required for structural analysis are as follows. The material is assumed to be a linear elastic MDF with E =4000 [MPa], Poisson's ratio $\nu = 0.25$, and density $\rho = 700$ [kg/m^3]. The thickness of the material is 2.0 cm. The kerf shape parameters are $n = 9$, $b = 0.1/n$ [m], and $h = 0.8/n$ [m]; this combination is above the allowable threshold in Fig. 3 and thus feasible. The kerf joints are modelled as zero-length springs whose 6-DoF stiffnesses are computed by the principle of virtual work, similarly to Eq. (9). The naked vertices of the equilateral triangular mesh in the flat state are pin-

supported. The deployed structure is subject to its self-weight. The number of face subdivisions is 3; i.e., each face is split into 9 sub-faces for precision of structural analysis. Geometric nonlinearity is not considered in this example. The structural analysis is implemented using Abaqus 2020.

The deformation of the single auxetic surface is shown in Fig. 5. The maximum displacement in the simulation is 183.6 m, which is excessively large, and the structure will easily break due to self-weight. Note that the maximum deformation without face subdivision is 183.2 m, which is close to the case in which the faces are subdivided. This is because the deformation energy is predominantly stored at the kerf joints, and face subdivision does not critically affect the structural analysis result.

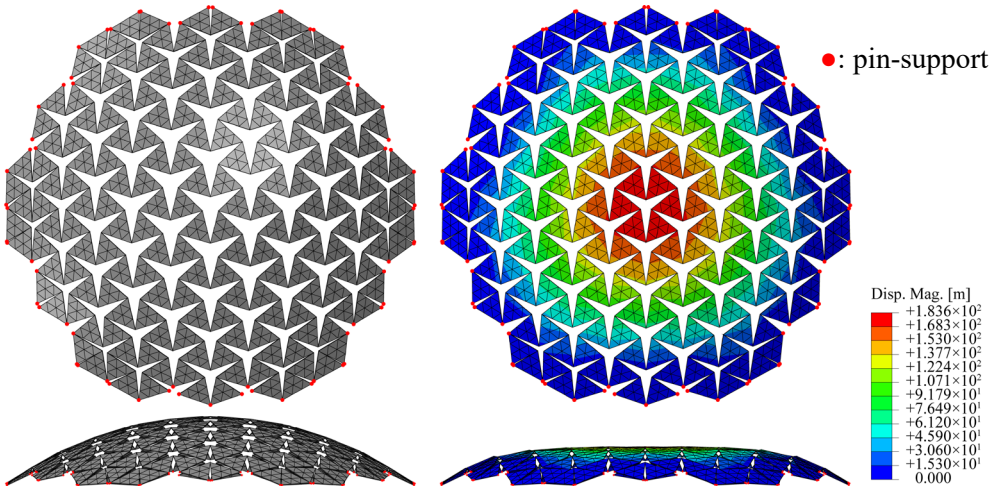

Figure 5: Initial shape of the single auxetic material for structural analysis (left) and deformed shape due to self-weight (right, deformation scale $\times\, 1/200$)

3.2.2. Stabilizing the deployed shape through overlaying

As described in the previous subsection, it is necessary to stiffen the deployed state to hold its shape against the restoring forces and self-weight. To address this problem, this study adopts the overlaying scheme, whose geometric aspects are clearly explained by Karunanidhi et al. [7] Inspired by this work, this subsection demonstrates the mechanical advantages of the overlaying scheme.

Figure 6 illustrates the basic concept of the overlaying scheme. In this scheme, the lower and upper layers are connected so that each pair of faces has opposite rotational directions for deployment. Then, the restoring forces cancel each other. Moreover, it increases the in-plane rotational stiffness, which was intentionally reduced by the kerf joints for deployment. Therefore, it can be expected to improve the stability of the entire structure.

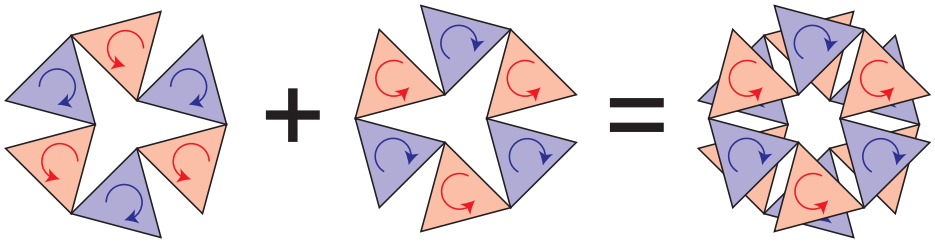

Figure 6: Conceptual diagram of the overlaying scheme. By overlaying two auxetic materials such that the connected faces have opposite rotational directions for deployment, the stiffness of the overlayed structure is expected to greatly increase.

As an example, consider connecting each pair of faces using 3 steel bolts as shown on the left of Fig. 7. Using the properties in Fig. 7 and the principle of virtual work, the 6-DoF stiffnesses of the equivalent spring element can be expressed as

$$\{K_{tx}, K_{ty}, K_{tz}, K_{rx}, K_{ry}, K_{rz}\} = \left\{\frac{3EA}{2t}, \frac{3GA_s}{2t}, \frac{3GA_s}{2t}, \frac{GA_s l^2}{2t}, \frac{EAl^2}{4t}, \frac{EAl^2}{4t}\right\} \tag{12a}$$

$$A_s = \frac{39}{44}A \tag{12b}$$

where K_{tx}, K_{ty}, and K_{tz} are the translational stiffnesses and K_{rx}, K_{ry}, and K_{rz} are the rotational stiffnesses in the local x, y, and z directions, respectively. Considering that the translational stiffnesses have a similar order of magnitude in Eq. (12a), they are roughly set to 2.0×10^8 [N/m]. Similarly, the rotational stiffnesses are set to 2.0×10^7 [N·m].

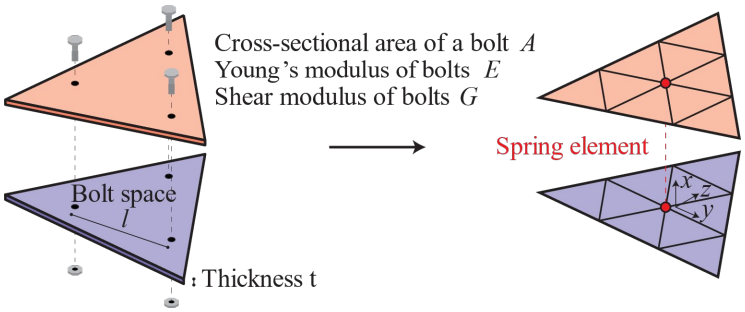

Figure 7: Conceptual diagrams of bolt connections for surface overlaying (left) and their equivalent spring element for structural analysis (right)

As shown on the right side of Fig. 7, the spring elements are modelled between the face centroids. To align face centroid and face subdivisions, the number of face subdivisions is recommended to be a multiple of 3. This is why the number of face subdivisions is 3 in the numerical examples. During structural analysis, there is no pin-support in the upper layer nodes.

The deformation of the bilayer auxetic surface is shown in Fig. 8. The maximum displacement in the simulation is 19.63 cm. Compared to the case of the single auxetic surface, the displacement is reduced by a factor of approximately 1000. which is a significant difference. While the deformation was concentrated in the central part in the case of the single auxetic surface, the entire surface is deformed in the bilayer case, demonstrating that the bilayer structure can transfer loads to the support more efficiently.

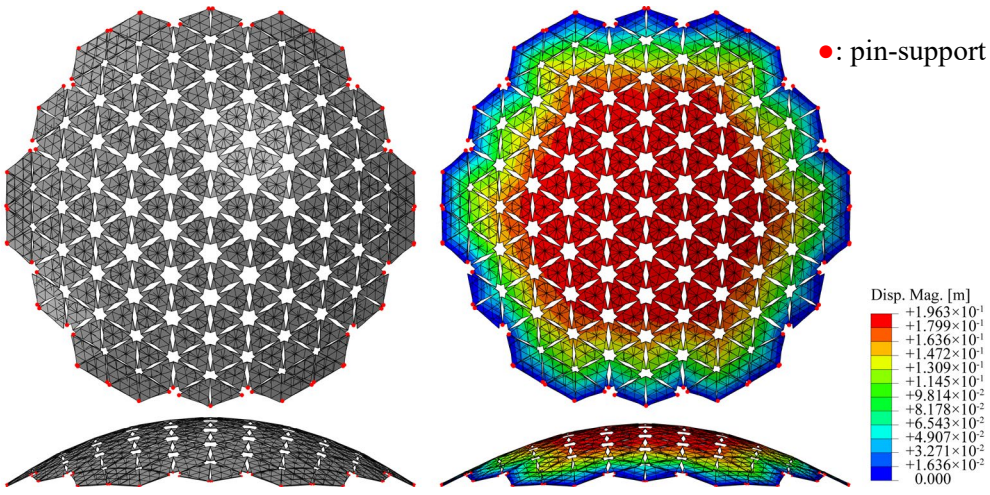

Figure 8: Initial shape of the bilayer auxetic material for structural analysis (left) and deformed shape due to self-weight (right, deformation scale × 1/1)

4. Design and analysis workflow for structural performance-aware auxetic materials

The overall workflow to design the auxetic materials incorporating kerf joints and surface overlaying is illustrated in Fig. 9. The workflow starts with defining the target surface. After conformal flattening with

Ricci flows, a conformal map and its corresponding conformal factors are obtained. At this point, the feasibility of the target shape must be verified by checking whether the conformal factors are within the admissible range $[0, \log 2]$. If not, the conformal factors should be shifted by uniformly scaling the conformal map or the target shape should be adjusted so as to have lower curvatures.

Equilateral triangles are tiled so as to approximate the shape of the conformal map. In this tiling step, the edge length is an important parameter that determines the complexity of the deployed shape. The deployment analysis is run for a pair of auxetic cut patterns. This way, the deployed shapes to be overlayed are obtained geometrically.

The next phase is creating the structural model for analysis. In addition to shell elements modelled onto the deployed shapes, it is necessary to design overlay joints and kerf joint shapes. These details are converted to 6-dof spring elements. To run structural analysis, it is also required to define the material thickness, material properties, boundary conditions, and load conditions.

Figure 10 shows examples of bilayer auxetic materials designed and analysed by the proposed workflow, which demonstrates the versatility of the proposed method. The initial shapes in Fig. 10 include negative Gaussian curvatures, and large displacements occur in those areas.

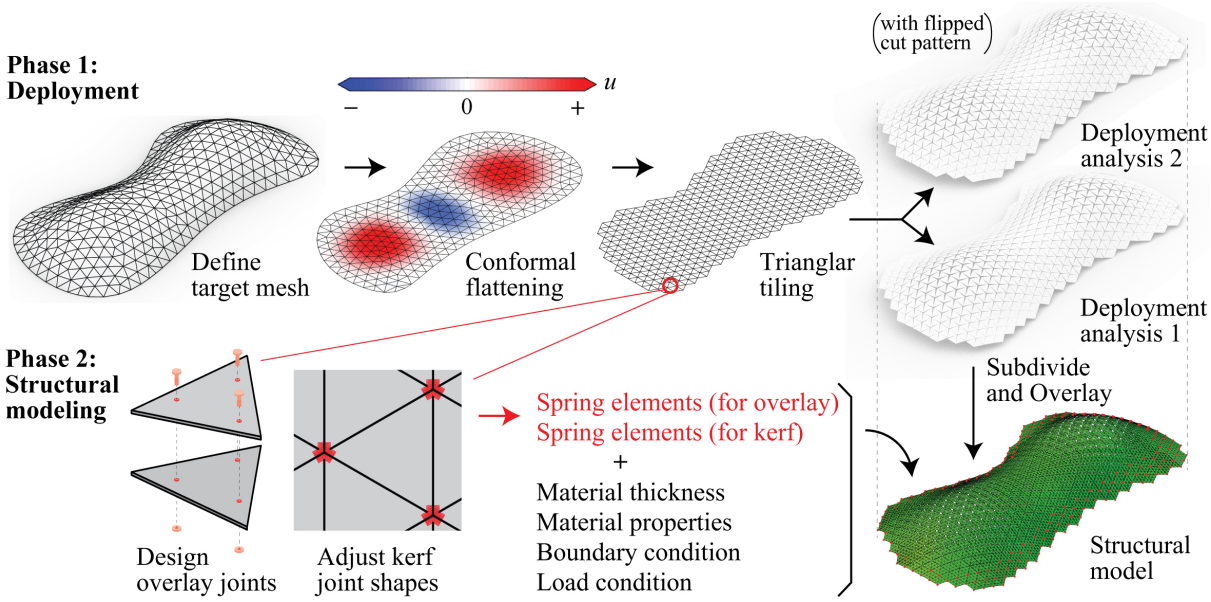

Figure 9: Proposed design workflow for bilayer auxetic materials with kerf joints

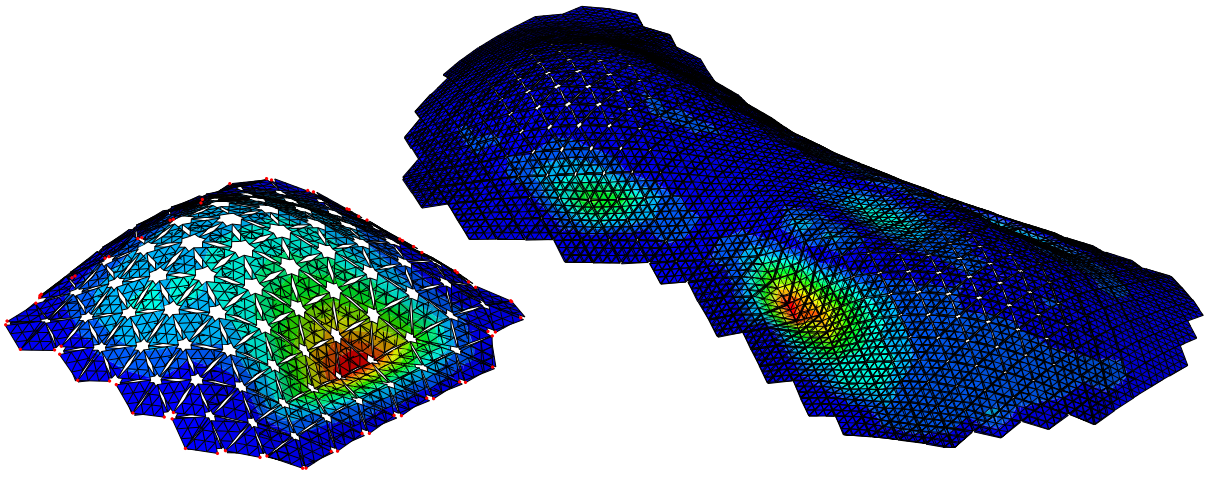

Figure 10: Examples of deformed bilayer auxetic materials with kerf joints. The color indicates the relative magnitude of nodal displacements subject to gravity, with red indicating large displacements.

5. Physical prototyping

As an extension of the design process, we created physical prototypes (single-layer and double-layer models) using laser-cut MDF with a thickness of 3 mm, as shown in Fig. 11. To the best of our knowledge, these prototypes are the first cut-processed auxetic structures made of a brittle material. Both models were designed to have an ellipsoid segment with a circular plan of 400 cm^2 and a height of 5.6 cm. The kerf parameters are set to $n = 5$, $h = 6.0$ [mm], and $b = 1.5$ [mm]. Each unit triangle contains three holes with a diameter of 1.6 mm. In connecting two layers, these holes are used for bolting with stainless steel screws (M1.6, 10 mm) and hex nuts (M1.6).

For the single-layer model without bolt connections, the maximum height of the middle surface is approximately 3.9 cm, indicating excessive flexibility. Still, the deformation against self-weight was much smaller than the simulation due to contact between adjacent triangles.

For the double-layer model, the maximum height of the middle surface is about 6.2 cm, demonstrating the stiffening effect of the double-layer scheme. There are three main reasons for the overheight: first, the model was roughly triangulated with an edge length of 4.5 cm; second, the deployed geometry is simply fixed by contact with the fixing element without considering that some parts of the outer triangles should be outside the circular domain; and finally, the panel thickness contributed to increasing the camber of surface in couple with the second reason.

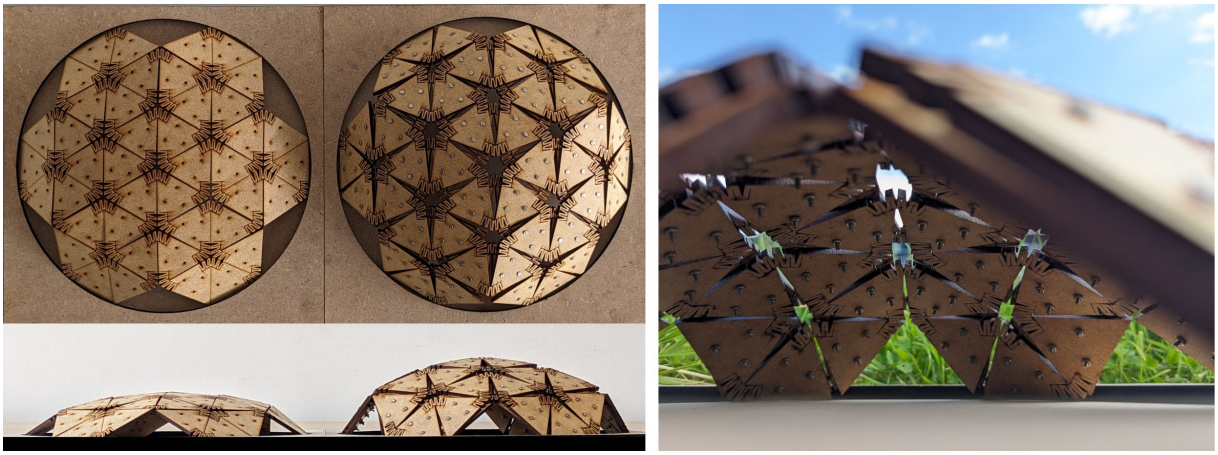

Figure 11: Prototypes created by the proposed design method. Resulting shapes of single-layer and double-layer models (left). Interior view of the double-layer model (right).

6. Conclusion

This study utilized kerf bending and surface overlaying to design relatively large-scale auxetic surface structures and quantitatively evaluated the effects of these improvements. Introducing kerf bending at the joints enables the material to be within the elastic range during the deployment process. The relationship between the kerf shape parameters and material properties is analytically obtained. From the relationship, it is found that wood materials can be used for auxetic structures by adjusting the kerf shape parameters. Through the numerical examples, the structure exhibits significant improvement in stiffness after surface overlaying, with a reduction of the maximum deformation by a factor of 1000.

However, the proposed design method has certain limitations, which include the following:

- This study uses the optimization method by Konaković et al. [4] for deployment simulation as it is, and the two deployed layers may not align well.
- This study does not consider cone singularity in the conformal flattening process. Thus, the design surface is limited to a surface with relatively low curvatures.
- Although the stiffness can be significantly improved owing to the overlaying scheme, it might not be sufficient to resist practical load scenarios, including dead and live loads.

- Introducing kerf joints may disrupt the geometrical relationship between the log conformal factor and the deployment angle, i.e., Eq. (4).
- Using thick materials may negatively affect the overlay-ability.
- Mechanical testing are necessary to appropriately choose the material and fabrication process.

Despite these limitations, the findings of this study offer promising insights into the potential of utilizing kerf bending and surface overlaying to enhance the structural properties of auxetic surface structures. Moreover, the developed design and analysis workflow is expected to make auxetic materials more accessible to architectural designers, structural engineers, and beyond.

Supplemental materials

The link to download the 3D spherical models used in this study is available at https://doi.org/10.5281/zenodo.11505501.

Acknowledgements

This research is supported by The Kajima Foundation Long-term Research Program, JSPS Grant No. 24K17392 and JST CREST Grant No. JPMJCR1911.

References

[1] M. Meloni, J. Cai, Q. Zhang, D. Sang-HoonLee, M. Li, R. Ma, T. E. Parashkevov, and J. Feng, "Engineering Origami: A Comprehensive Review of Recent Applications, Design Methods, and Tools, " Advanced Science, vol. 8, no. 13, 2021.

[2] Cheng Wang, Jun-lan Li, Da-wei Zhang, "Optimization design method for kirigami-inspired space deployable structures with cylindrical surfaces, " *Applied Mathematical Modelling*, vol. 89, pp. 1575-1598, 2021.

[3] D. Wood, P. Grönquist, S. Bechert, L. Aldinger, D. Riggenbach, K. Lehmann, M. Rüggeberg, I. Burgert, J. Knippers, and A. Menges, “From machine control to material programming: Self-shaping wood manufacturing of a high performance curved CLT structure -- Urbach Tower," in Burry, J., Sabin, J., Sheil, B., Skavara, M. (eds.), *Fabricate 2020: Making Resilient Architecture*, UCL Press, pp. 50-57, 2020.

[4] M. Konaković, K. Crane, B. Deng, S. Bouaziz, D. Piker, and M. Pauly, "Beyond developable: computational design and fabrication with auxetic materials," *ACM Transactions on Graphics*, vol. 35, no. 89, pp. 1-11, 2016.

[5] Y. Sakai and M. Ohsaki, "Optimization method for shape design of auxetic bending-active gridshells using discrete differential geometry," *Structures*, vol. 34, pp. 1589-1602, 2021.

[6] D. Mitov, B. Tepavčević, V. Stojaković, and I. Bajšanski, "Kerf Bending Strategy for Thick Planar Sheet Materials," *Nexus Network Journal*, vol. 21, pp. 149–160, 2019.

[7] N. K. Karunanidhi, M. Sobczyk, S. Wiesenhütter, T. Wallmersperger, and J. R. Noennig, "Programmable multi-layered auxetic mechanisms," *Journal of Materials Science*, vol. 58, pp. 13253-13268, 2023.

[8] Y.-L. Yang, R. Guo, F. Luo, S.-M. Hu, X. Gu, "Generalized Discrete Ricci Flow," *Computer Graphics Forum*, vol. 28, no. 7, pp. 2005–2014, 2009.

[9] C. Douthe, J. F. Caron, O. Baverel, "Gridshell structures in glass fibre reinforced polymers," *Construction and Building Materials*, vol. 24, pp. 1580–1589, 2010.

[10] A. Syamsir, A. H. Amat, F. Usman, Z. Itam, N. L. M. Kamal, N. M. Zahari, M. Chairi, and R. Imani, "Effect of fiber orientation on ultimate tensile strength and young’s modulus of fabricated glass fiber reinforced polymer plates," in *Proceedings of Green Design and Manufacture 2020*, *Construction and Building Materials*, vol. 2339, no. 1, 2021.